Unclassified

AD-A203 355

DOCUMENTATION PAGE

Form Approved
OMB No. 0704-0188

DTIC FILE COPY

1b RESTRICTIVE MARKINGS

2a. SECURITY CLASSIFICATION AUTHORITY

3. DISTRIBUTION/AVAILABILITY OF REPORT
Approved for public release:
Distribution is Unlimited

2b. DECLASSIFICATION/DOWNGRADING SCHEDULE

4. PERFORMING ORGANIZATION REPORT NUMBER(S)
NA

5. MONITORING ORGANIZATION REPORT NUMBER(S)
NA

6a. NAME OF PERFORMING ORGANIZATION
Univ. of North Texas

6b. OFFICE SYMBOL (If applicable)

7a. NAME OF MONITORING ORGANIZATION
Center for Night Vision and Electro-Optics

6c. ADDRESS (City, State, and ZIP Code)

7b. ADDRESS (City, State, and ZIP Code)
ATTN: AMSEL-RD-NV-IRT
Fort Belvoir, VA 22060-5677

8a. NAME OF FUNDING/SPONSORING ORGANIZATION
CNVEO

8b. OFFICE SYMBOL (If applicable)
AMSEL-RD-NV-IT

9 PROCUREMENT INSTRUMENT IDENTIFICATION NUMBER
DAAB07-87-C-F094

8c. ADDRESS (City, State, and ZIP Code)
Fort Belvoir, VA 22060-5677

10. SOURCE OF FUNDING NUMBERS

PROGRAM ELEMENT NO.	PROJECT NO.	TASK NO	WORK UNIT ACCESSION NO
661102A	1L161102A31B	H0	007-CJ

11. TITLE (Include Security Classification)
Two Photon Characterization

12. PERSONAL AUTHOR(S)
David G. Seiler

13a. TYPE OF REPORT	13b. TIME COVERED	14. DATE OF REPORT (Year, Month, Day)	15. PAGE COUNT
Interim	FROM 2/88 TO 5/88	12/88	22

16. SUPPLEMENTARY NOTATION

17. COSATI CODES			18. SUBJECT TERMS (Continue on reverse if necessary and identify by block number)
FIELD	GROUP	SUB-GROUP	
17	05		Defect characterization; Magneto-Optical measurements; Two Photon Spectroscopy; Narrow band gap semiconductors, II-VI compounds.

19. ABSTRACT (Continue on reverse if necessary and identify by block number)

Magneto-Optical studies of HgCdTe have provided a rich new group of spectroscopies for studying defects and impurities in narrow band semiconductors such as HgCdTe.

20. DISTRIBUTION/AVAILABILITY OF ABSTRACT	21. ABSTRACT SECURITY CLASSIFICATION
☐ UNCLASSIFIED/UNLIMITED ☒ SAME AS RPT. ☐ DTIC USERS	Unclassified

22a. NAME OF RESPONSIBLE INDIVIDUAL	22b TELEPHONE (Include Area Code)	22c. OFFICE SYMBOL
Frederick F. Carlson	703-664-5036	AMSEL-RD-NV-IT

DD Form 1473, JUN 86 — Previous editions are obsolete

SECURITY CLASSIFICATION OF THIS PAGE
Unclassified

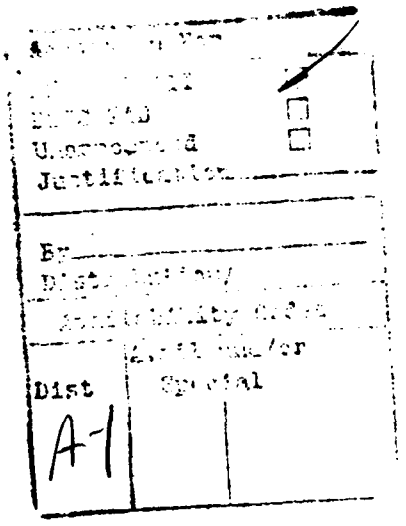

Performance Report

February 28, 1987 - May 27, 1988

Third Quarter (Three Months)

Contract DAAB07-87-C-FO94

With U. S. Army Night Vision and Electro-Optics Center

Fort Belvoir, Virginia 22060-5677

Contract Monitor: Dr. Fred Carlson

"Two-Photon Absorption Characterization"

Principal Investigator: Dr. David G. Seiler

Center for Applied Quantum Electronics

Department of Physics

University of North Texas

Denton, Texas 76203

Performance Report
February 28, 1988 - May 27, 1988
Third Quarter (Three Months)
Contract DAAB07-87-C-FO94

"Two-Photon Absorption Characterization"

P.I., Dr. David G. Seiler
University of North Texas

According to the Time Phase Task Schedule for the third quarter on p. 26 of the proposed Technical Work, our research investigation and sample characterization has proceeded along four task categories (b), (c), (f), and (e):

(b) Investigate two-photon absorption...

(c) Identify impurity related energy levels and correlate...

(e) Investigate time resolved behavior in HgCdTe excited by two-photon absorption. Estimate the lifetimes of charge carriers.

(f) Analyze "lifetime" data to determine surface and bulk recombination probabilities.

We shall now address the progress in each of the tasks.

I. (b) Investigate two-photon absorption

As pointed out in the last quarter, a major breakthrough was achieved in observing two-photon magnetoabsorption (TPMA) in bulk samples of both n- and p-type $Hg_{1-x}Cd_xTe$. During this quarter, a major emphasis was placed on data interpretation. We now present TPMA results and analyses on four different samples of HgCdTe with different x-values (n-type samples of x = 0.238, 0.258, 0.276).

n - HgCdTe(x = 0.236)

This sample was obtained from Honeywell and had the following properties:

$$\mu(77K) = 1.6 \times 10^5 cm^2/Vsec$$

$$n(77K) = 1.4 \times 10^{14} cm^{-3}$$

Infrared transmission x = 0.2406 ± 0.001

Figure 1 shows the photoconductive (PC) response of the sample versus magnetic field B for various CO_2 laser wavelengths. A variety of resonant structure is observed which we shall now describe in detail.

Table I. Two-Photon Magneto Absorption Transitions for $Hg_{1-x}Cd_xTe$ Given From Low Energy to Higher Energies.

Designation	Energy Level Transition	Polarization
R_1	$a^-(2) \rightarrow a^c(0)$	σ_R
R_2	$b^-(2) \rightarrow b^c(0)$	σ_R
π_1	$a^+(0) \rightarrow a^c(0)$	π or σ
L_1	$a^+(-1) \rightarrow a^c(1)$	σ_L
π_2	$a^-(1) \rightarrow a^c(1)$	π or σ
R_3	$a^-(3) \rightarrow a^c(1)$	σ_R
π_3	$b^-(1) \rightarrow b^c(1)$	π or σ
L_2	$b^+(-1) \rightarrow b^c(1)$	σ_L
π_4	$b^+(0) \rightarrow b^c(0)$	π or σ
π_5	$a^-(2) \rightarrow a^c(2)$	π or σ
π_6	$b^-(2) \rightarrow b^c(2)$	π or σ
R_4	$a^+(2) \rightarrow a^c(0)$	σ_R
L_3	$a^+(0) \rightarrow a^c(2)$	σ_L
π_7	$a^+(1) \rightarrow a^c(1)$	π or σ
π_8	$a^-(3) \rightarrow a^c(3)$	π or σ
L_4	$b^+(0) \rightarrow b^c(2)$	σ_L

The notation is as follows:

a, b denote different spin states; the superscript - (+) denotes a heavy hole state (light hole state); the superscript c denotes a conduction band state.

First of all, some of the structure in Fig. 1 have resonances whose magnetic field position depend upon the laser wavelength or photon energy. One example of this is shown by the arrow marked in the Figure. We identify this structure as arising from two-photon absorption transitions that take an electron from an initial hole Landau level (E_H) to a final conduction band Landau level (E_C). Possible transitions are given in Table I. Comparisons between the TPA and theoretical predictions are shown in Fig. 2 where $2\hbar\omega$ is plotted versus B. The lines represent the theoretical variation calculated from $2\hbar\omega = E_C - E_H$, where the Landau level energies are calculated with a modified Pidgeon-Brown energy band model using the following set of band parameters:

$$E_p = 19.0 \text{ eV}, \Delta = 1.0 \text{ eV}$$

$$\gamma_1 = 3.3, \gamma_2 = 0.1, \gamma_3 = 0.9$$

$$F = -0.8,\ N_1 = 0,\ \kappa = -0.8.$$

These are the set of parameters given by Weiler in her Semiconductors and Semimetal article.[1] The energy gap was then adjusted to give the "best fit" to the observed transitions. Excellent agreement is attained with $E_g = 121.8 \pm 0.5$ meV which corresponds to an x-value of 0.2363 ± 0.0003 using the Hanson, Schmit, Casselman relationship to relate x to E_g.[2]

The excellent agreement between the data and the two-photon transition energy theoretical variations are one of the strongest evidences that these observed transitions are indeed two-photon related. Further proof as to this designation comes from polarization studies shown in Fig. 3 obtained using an infrared zero order wave plate that converts linear polarized light into either left (σ_L) or right (σ_R) circularly polarized light. These data were taken on a sample obtained from Texas Instruments (it had a similar x-value to the Honeywell sample). The strongest (TPA) transitions occur for σ_L polarization as expected. These two σ_L transitions seem to be the distinguishing feature of the two-photon spectra in $Hg_{1-x}Cd_xTe$. Two-photon spectra observed in InSb are quite different as seen by the data in Fig. 4. for $T \approx 50K$ and $\lambda = 9.23$ μm. Note the much sharper linewidths and the wide variety of structure. The very broad linewidths of HgCdTe are due to inhomogeneities. This fact can be used to quantitatively estimate the amount of inhomogeneity broadening from the width of the resonance peaks.

Some of the structure (10.5 μm to 10.79 μm) present in Fig. 1 is independent of laser wavelength. We shall comment on this structure later in the report.

Other absorption processes occur at lower magnetic fields and lower wavelengths as seen in Fig. 5. Two additional absorption mechanisms occur - one-photon interband absorption (OPA), and absorption due to electron transitions from a shallow acceptor to the lowest conduction band Landau level. These transitions occur at much lower intensities than the TPA transitions. The temperature dependence of the PC response at 9.69 μm is shown in Fig. 6. As can be seen, the impurity transition becomes much weaker at the higher temperatures. Verification of these identifications comes from the good agreement between the theoretically calculated one-photon transition energies and the experimental data as shown in Fig. 7. The one-photon transition energies are given by

$$\hbar\omega_{OPA} = E_c - E_v \text{ (interband, with no exciton corrections)}$$

and

$$\hbar\omega_{IMP} = E_c - E_a \text{ (impurity)}$$

With an energy zero at the top of the valence band, at $B = 0$, $E_v = 0$ and $\hbar\omega_{OPA} - \hbar\omega_{IMP} = E_a =$ the acceptor impurity binding energy. The best fit to the data gives $E_a = 9.0$ meV.

Figure 8 shows the intensity dependence of the PC response at $T = 7$ K and $\lambda = 10.20$ μm, a wavelength where all three absorption mechanisms can be seen. First of all, at much lower intensities than used in Fig. 8 only OPA structure can be seen. As the intensity is increased to $I_0/4$, TPA structure can be seen at very high fields and the acceptor impurity structure becomes larger than the OPA structure which saturates at these high intensities. Finally, at the highest intensity, $I_0 = 1.8$ kW/cm^2, only the impurity and TPA structure can be observed.

The intensity dependence of the PC response at $T = 6$ K and $\lambda = 9.29$ μm, the region of the OPA and impurity structure is shown in Fig. 9. At low intensities only OPA structure dominates. At the highest intensity shown in Fig. 9, some unusual structure is observed at fields smaller than the highest field OPA structure. The photon energy dependence of these new transitions is shown in Fig. 10 on an expanded, more sensitive B-field scale. We note that the resonant positions of this structure do not depend greatly upon wavelength. During the next quarter, we shall work on interpreting this structure. For now we just note that it is there.

n - HgCdTe (x - 0.256)

This bulk sample was obtained from Cominco and had the following properties:

300 K
IR-TCO

x min = 0.258
x max = 0.261

μ = 7.3 x $10^3 cm^2/V.sec$
n = 7.2 x $10^{15} cm^{-3}$

77 K
μ = 7.6 x $10^4 cm^2/V.sec$
n = 1.0 x $10^{14} cm^{-3}$

Crystal identification p4100.60

Figure 11 shows TPA spectra in the PC response for this sample at 7K. The dominant features are again two resonant absorption processes seen at high fields. Good agreement between the calculated two-photon transition energies vs. B field and the experimental data is obtained for E_g = 156.0 ± 0.5 meV or x = 0.2580 ± 0.0003 as seen in Fig. 12.

The half-width of the resonant TPA structure can be used to determine the amount of inhomogeneity due to an x-value variation. As stated earlier, the TPA linewidths in n-InSb are much narrower (factor of 10) than in HgCdTe. Homogeneous samples of HgCdTe would have one x-value. Variations in x-value lead to variations in E_g. Thus, if one determines the field positions of the full width at half-maximum of the resonances, these can be used to calculate values of E_g or hence x. Figure 13 shows the experimental data for these half maximum positions for the two main transitions seen in Fig. 11. These in turn are fit to theoretical calculations with upper (160 meV) and lower (152 meV) values. This leads to an x-variation of ΔX = 0.0025.

n - HgCdTe (x = 0.277)

This bulk sample was obtained from Cominco and it had the following properties:

300 K
IR-TCO

x min = 0.276
x max = 0.278

μ = 5.8 x $10^3 cm^2/V.sec.$
n = 5.2 x $10^{15} cm^{-3}$

77 K
μ = 6.6 x 10^4
n = 1.4 x 10^{14}

Crystal identification 15(603) - 51

Two-photon structure is again observed in the PC response of this sample as seen in Fig. 14. Two main features dominate as before, with two additional much broader resonances occurring at higher fields. The fan chart of 2 $\hbar\omega$ vs. B in Fig. 15 shows a comparison between the data and the calculated transitions. The two main transitions are clearly in excellent agreement with the calculations demonstrating that they are related to TPA structure. However, the high field structure can not be explained by any known two-photon transitions. The three that are possible, R_1, R_2, and π_1

show rather strong disagreement with the data. Consequently, we believe that the most plausible interpretation of this structure is that they arise from electron transitions from two separate midgap levels to the lowest conduction band Landau level $a^c(0)$. The deep level energies would not depend on magnetic field and so the transition energy would be

$$\hbar\omega = E(a^c(0)) - E_d$$

which would be governed by the variation of $E(a^c(0))$. In Fig. 16, $\hbar\omega$ is plotted versus B showing the excellent agreement between the data and the theoretically calculated variation using E_d values of Ed_1 = 100 meV and Ed_2 = 94 meV. We note that midgap levels in HgCdTe are expected and these measurements are an important indication of their presence and provide an accurate determination of their location.

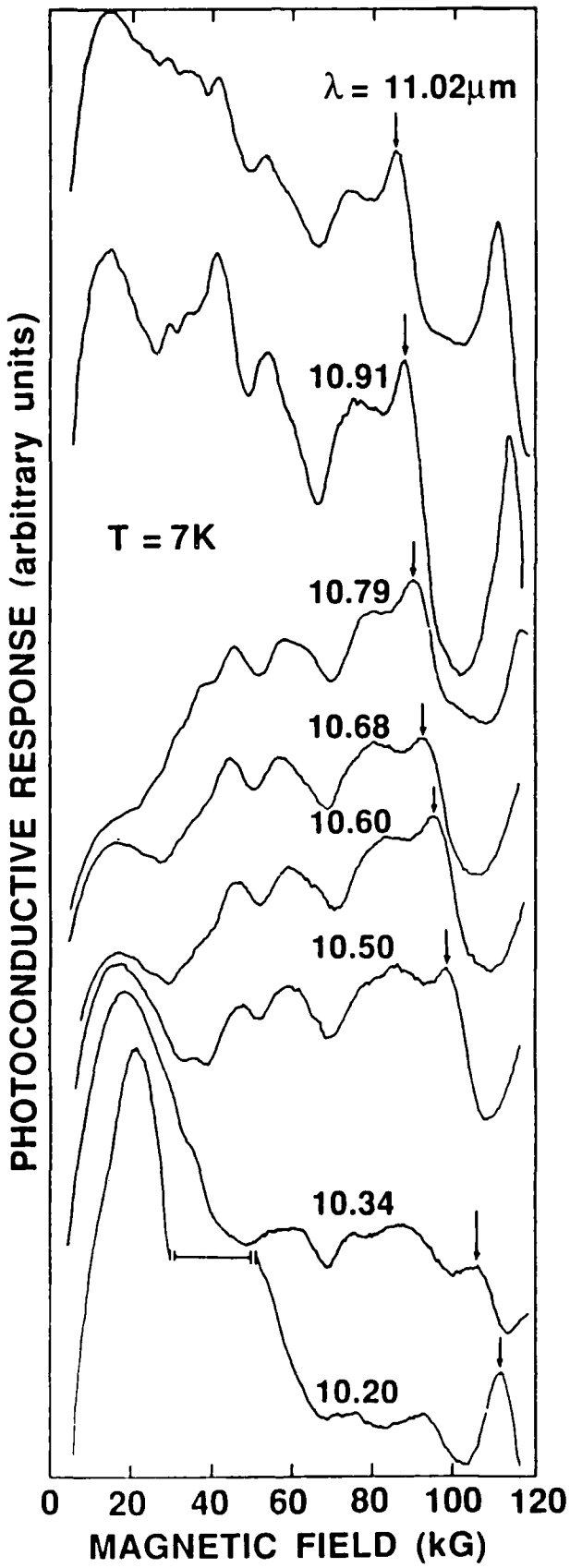

Figure 1. Wavelength dependence of photoconductive response showing high intensity structure.

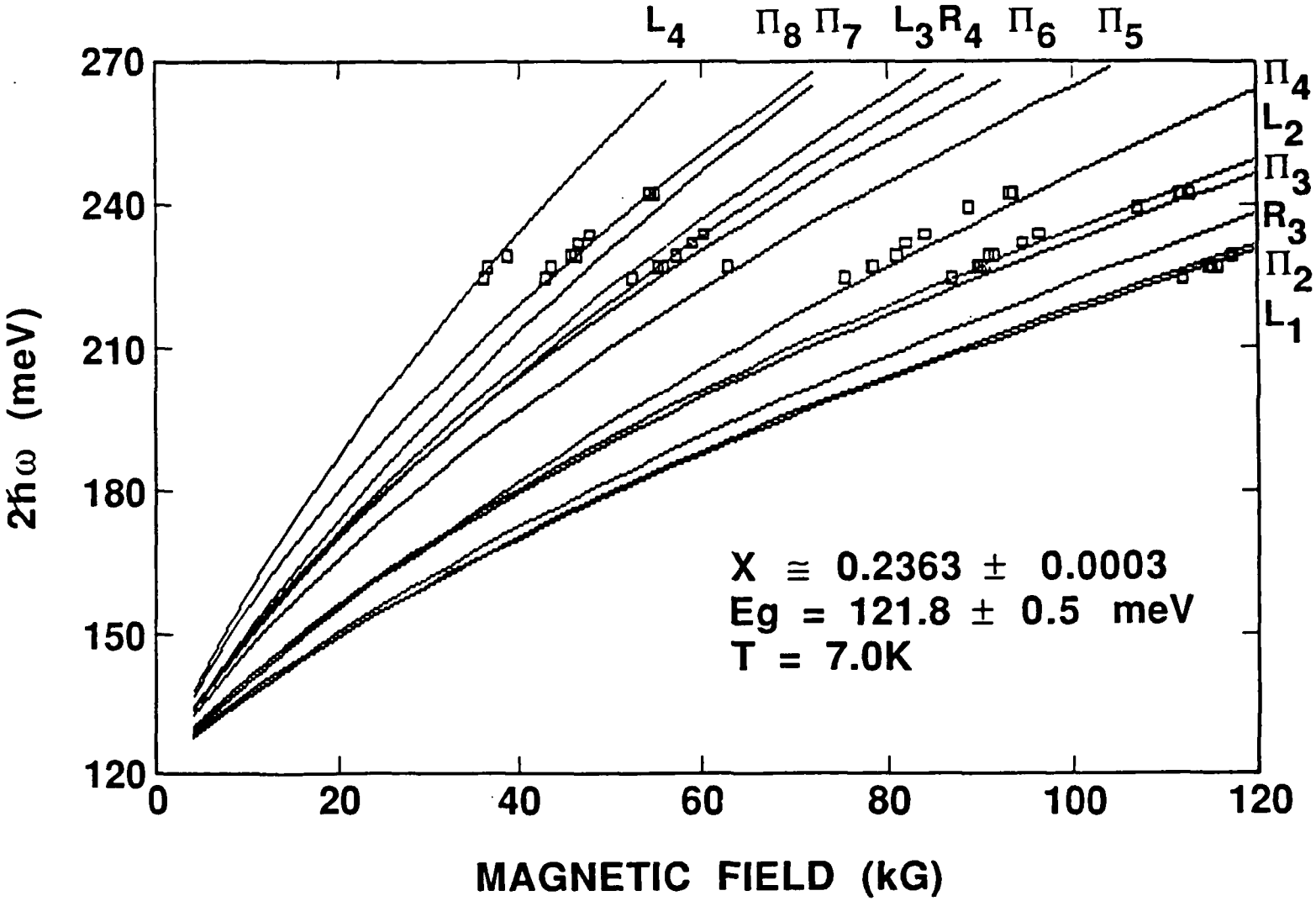

Figure 2. Fan chart of transition energy vs. magnetic field. The lines are theoretical energies calculated from a modified Pidgeon-Brown model. They extrapolate at zero field to the band gap (121.8 meV). The labels for each transition represent the polarization of the incident light, and the energetic order.

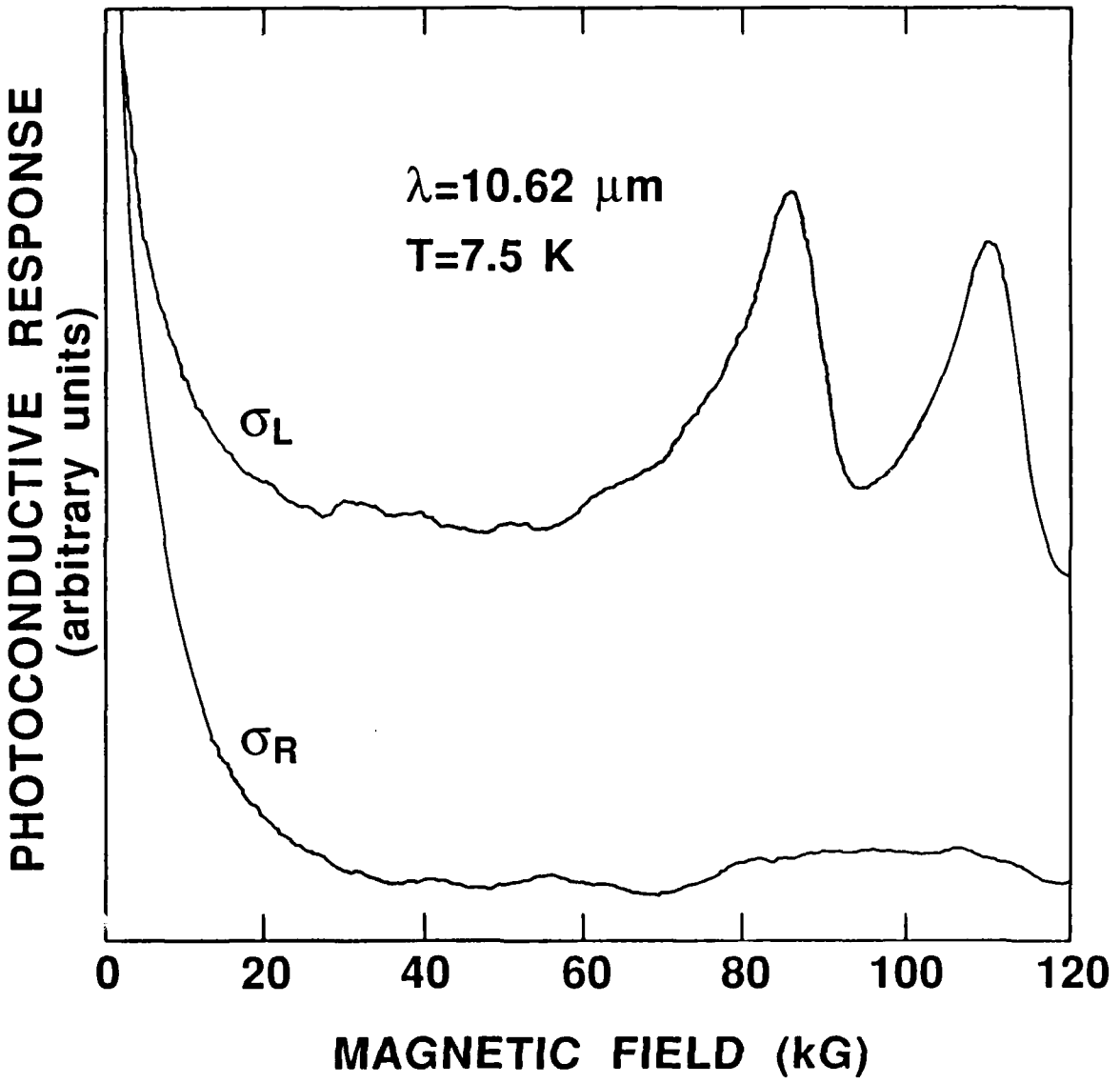

Figure 3. Polarization dependence of the photoconductive response showing clearly that the two dominant transitions arise from left circular polarization.

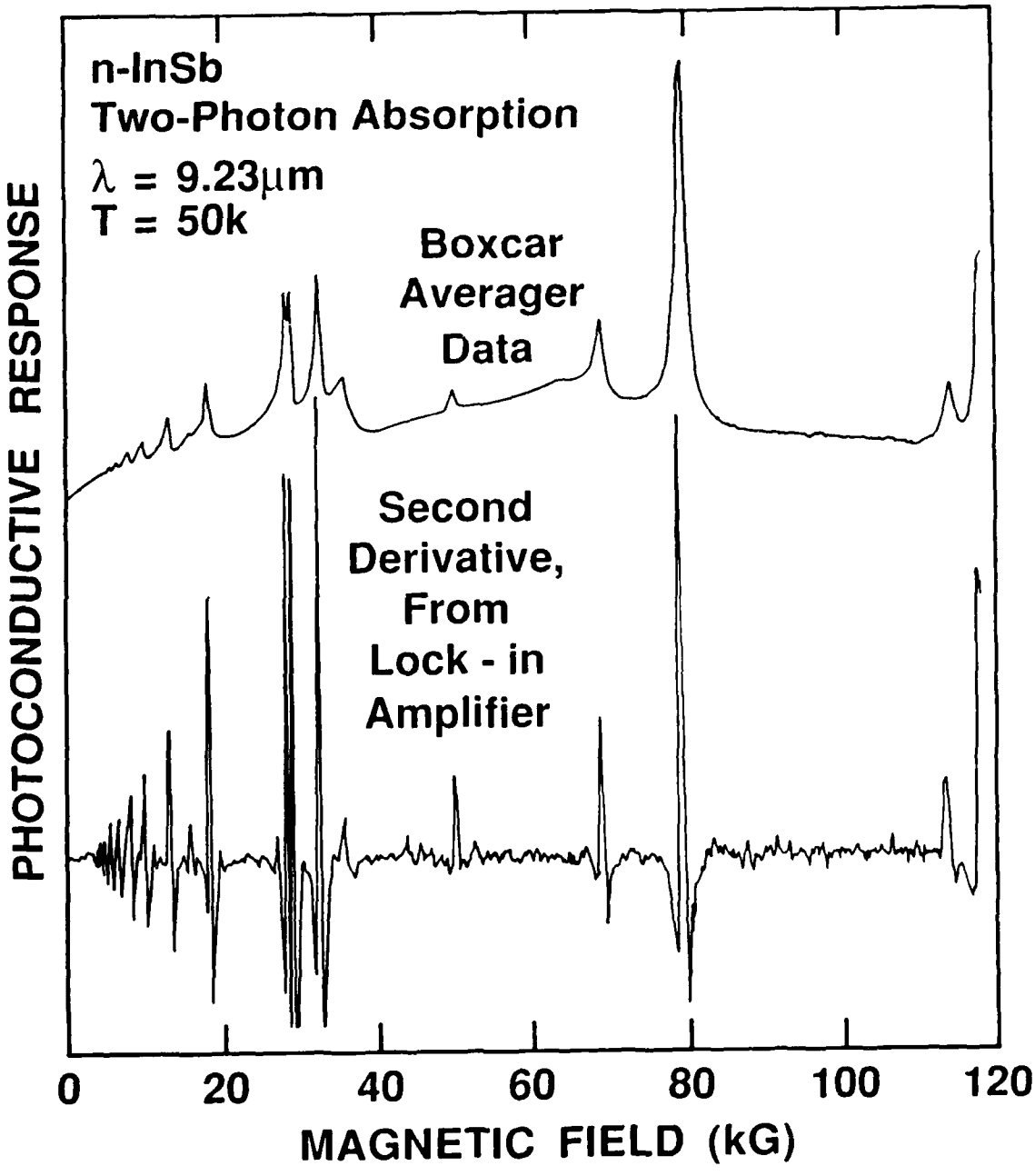

Figure 4. Two photon absorption spectra in n-InSb. The upper trace was analyzed with a boxcar averager, the lower with lock-in amplifier techniques which synthesize the second derivative.

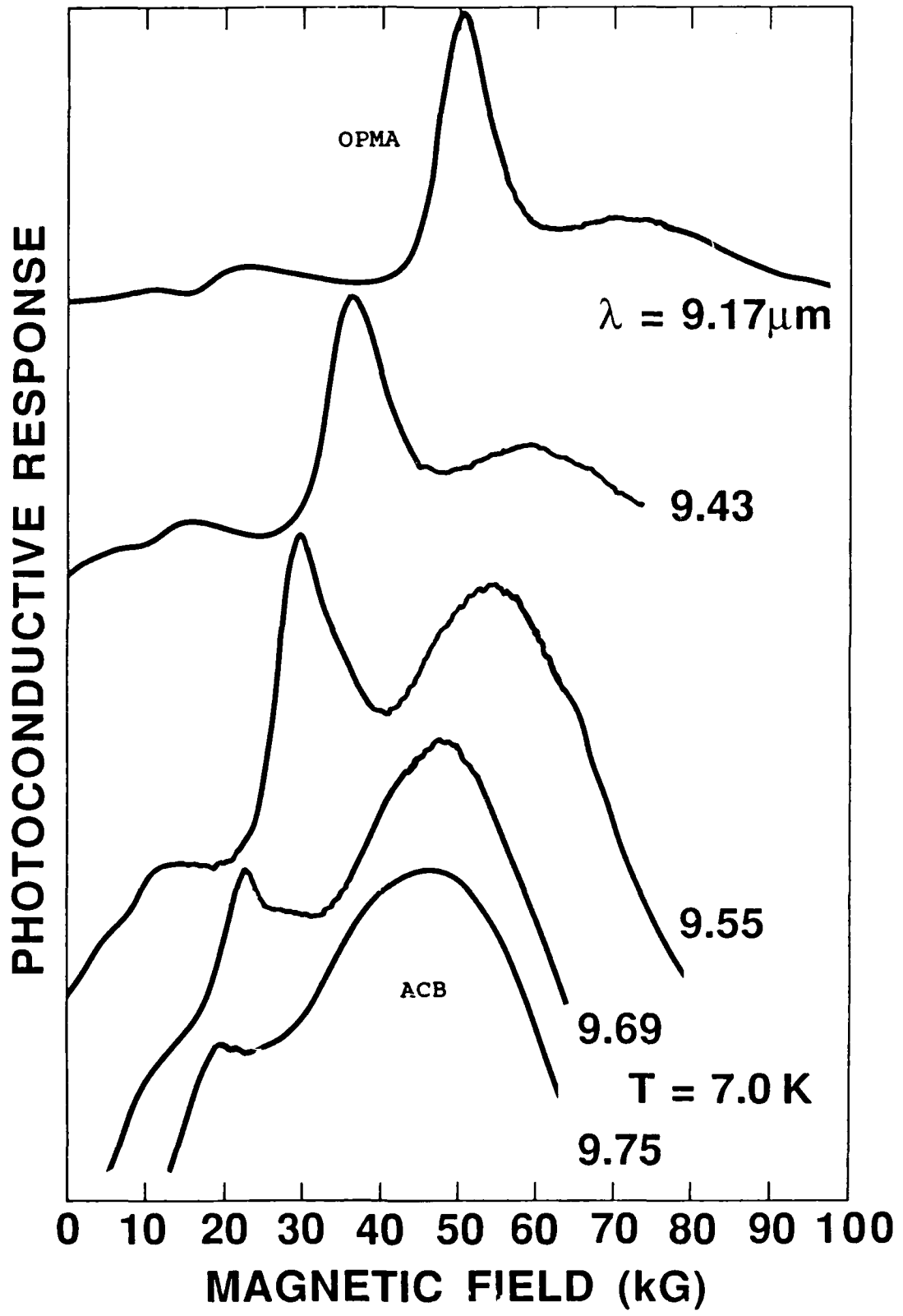

Figure 5. Wavelength dependence of the photoconductive response in HgCdTe. One photon magneto-absorption (OPMA) and acceptor to conduction band (ACB) transitions are shown.

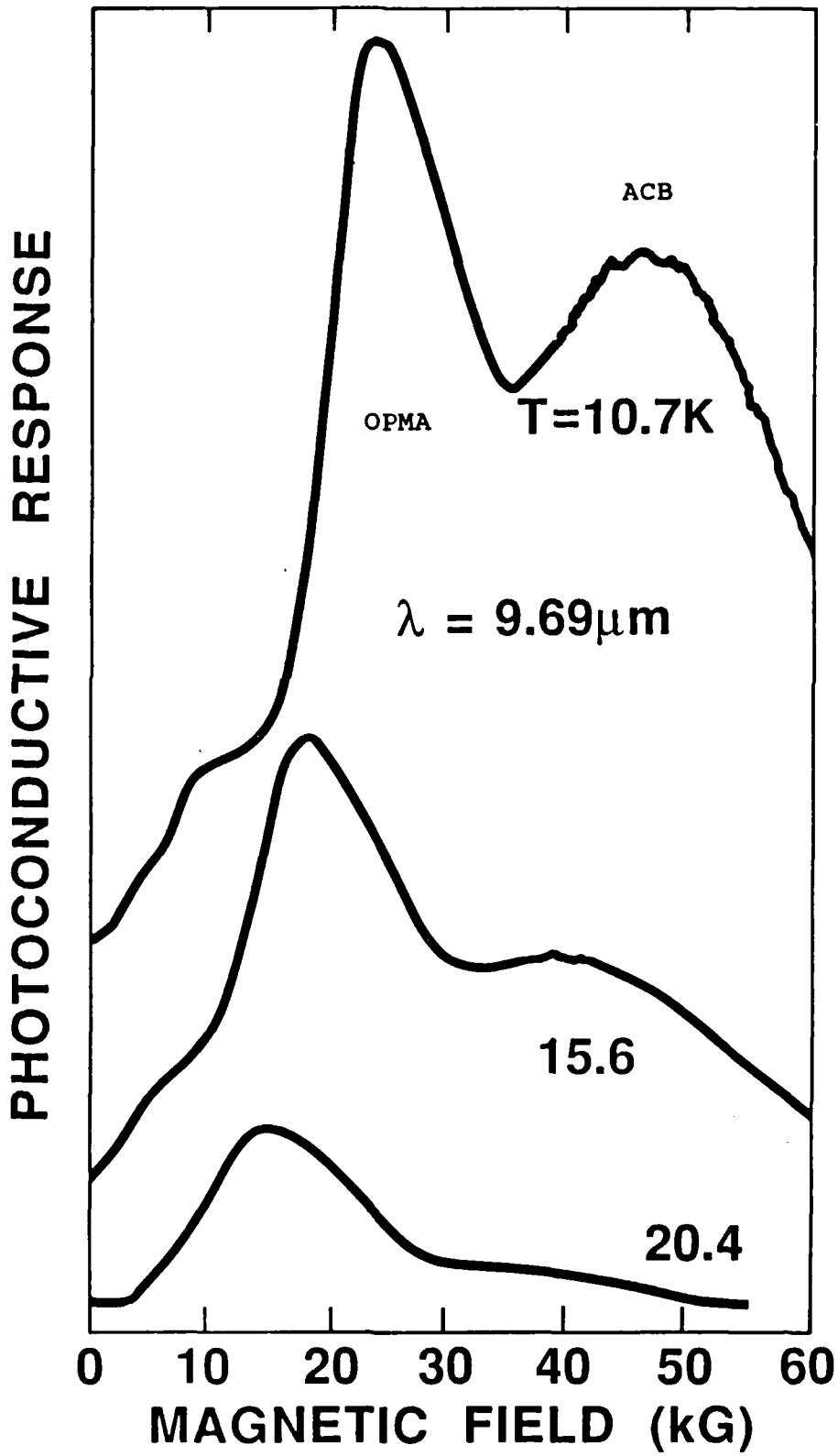

Figure 6. Temperature dependence of the photoconductive response of HgCdTe. Note that the ACB structure is more strongly temperature dependent than is the OPMA structure.

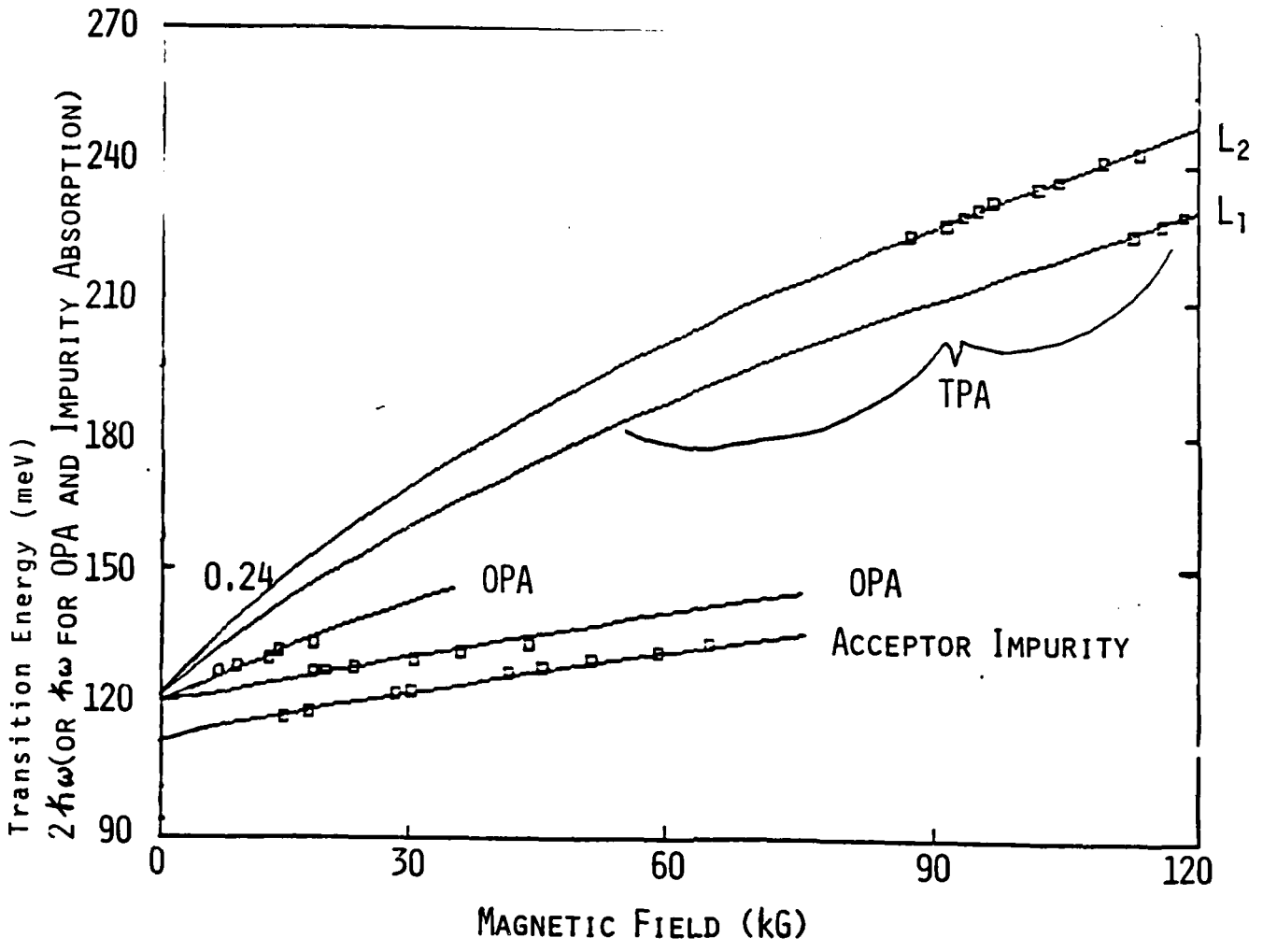

Figure 7. Fan chart of transition energies vs. magnetic field for HgCdTe. One-photon absorption (OPA), two-photon absorption (TPA), and acceptor to conduction band (Acceptor Impurity) transitions are shown.

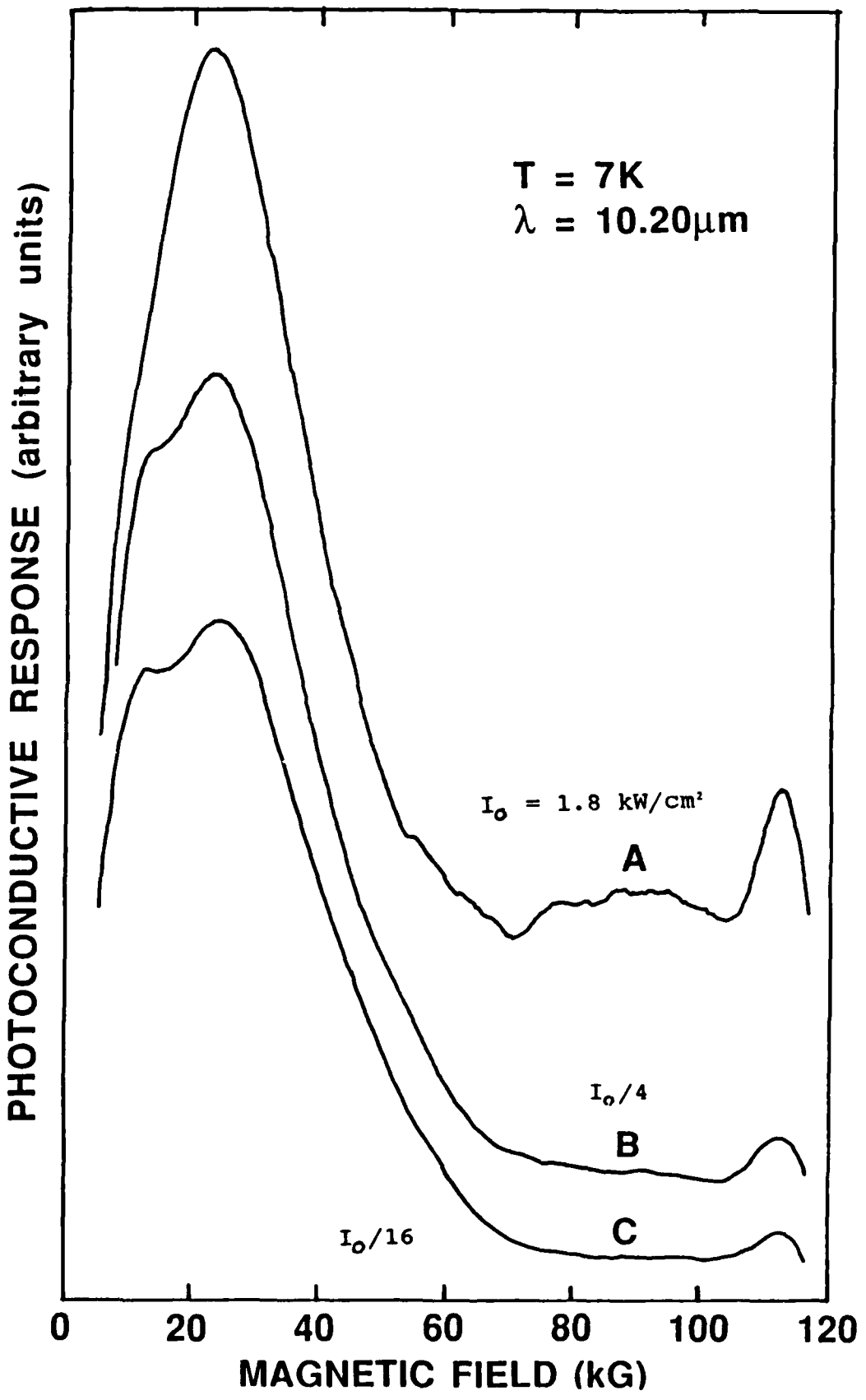

Figure 8. Photoconductive response of HgCdTe for various incident photon intensities. Note the damping out of the two-photon absorption (TPA) structure with decreasing intensity, and the seperation of the impurity and one-photon absorption structures.

Figure 9. Incident photon intensity dependence of the photoconductive response of HgCdTe showing high intensity structure, acceptor to conduction band (ACB) structure, and one-photon magneto absorption (OPMA) structure.

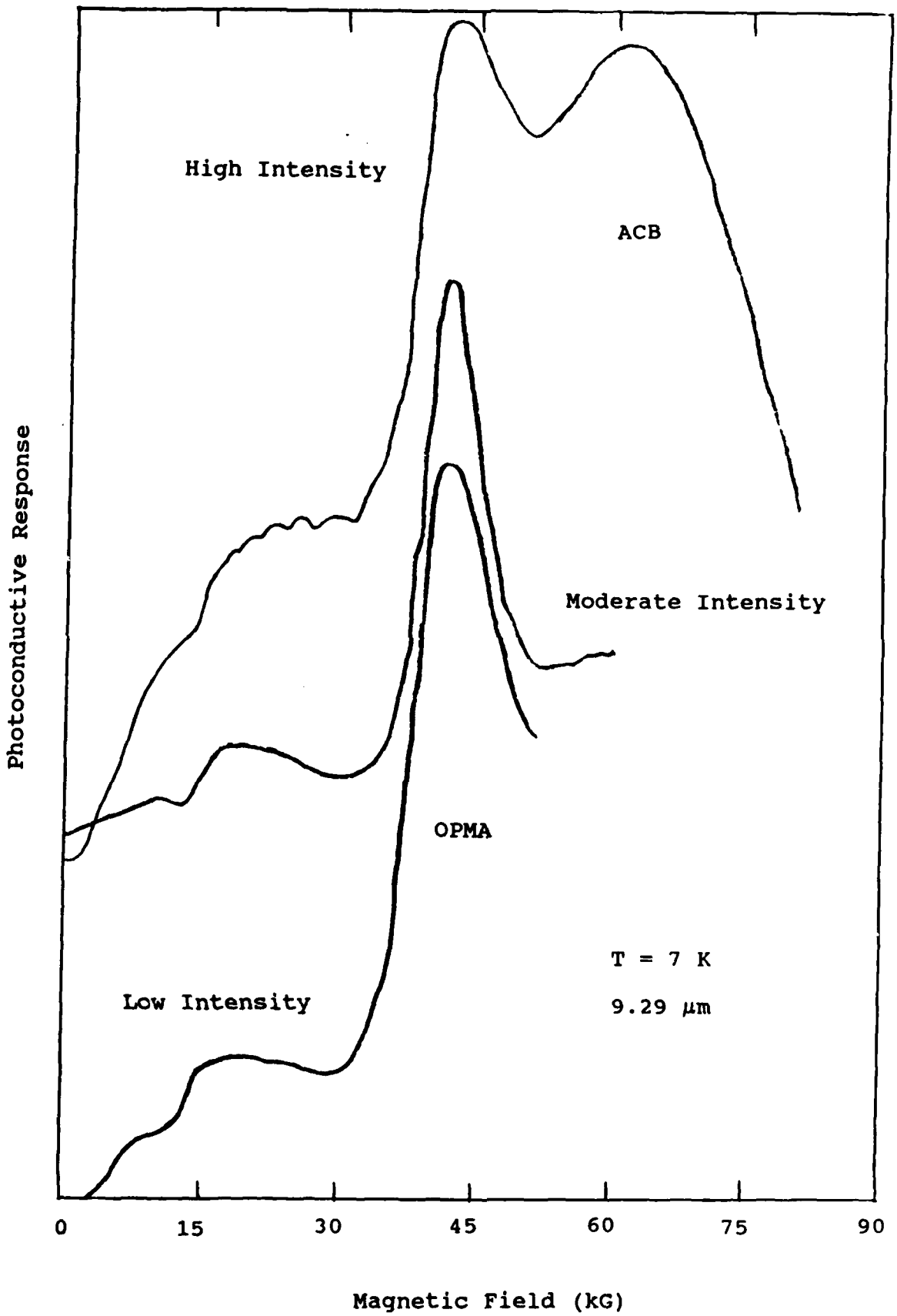

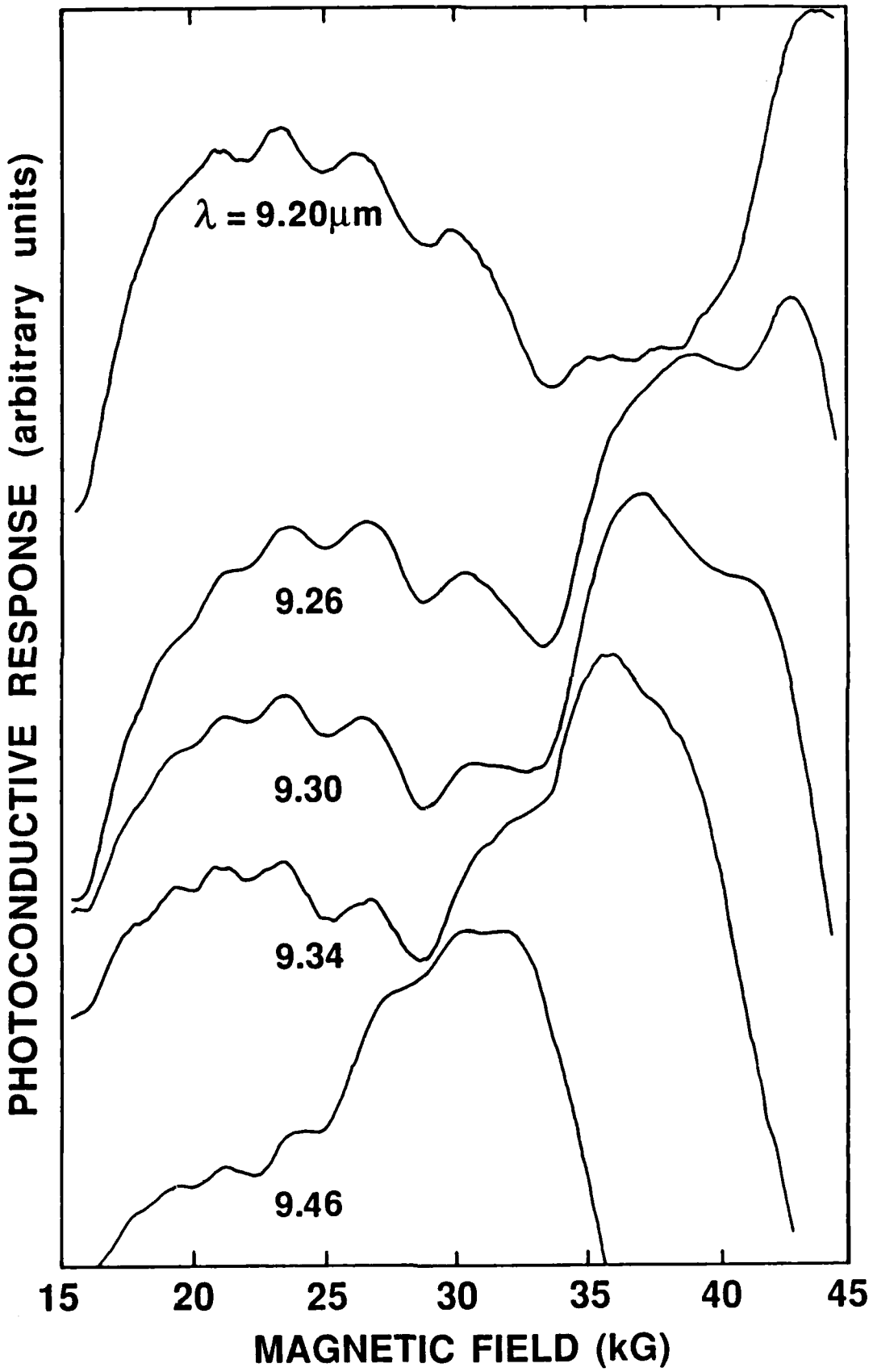

Figure 10. Wavelength dependence of the high intensity structure showing the movement of the one-photon magneto absorption (OPMA) structure against the high intensity structure.

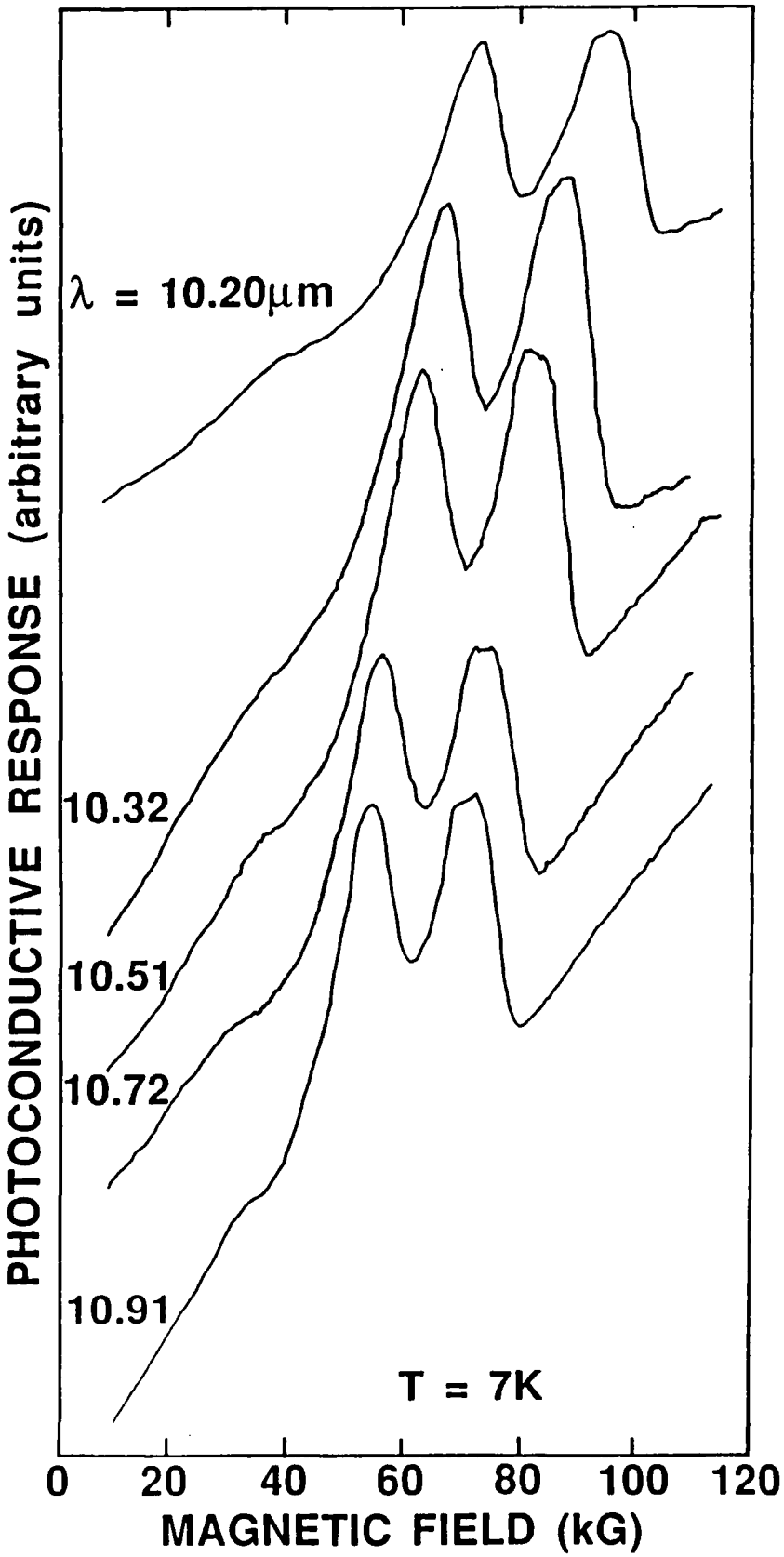

Figure 11. Wavelength dependence of the dominant two-photon magneto absorption (TPMA) structure in HgCdTe with x = 0.26.

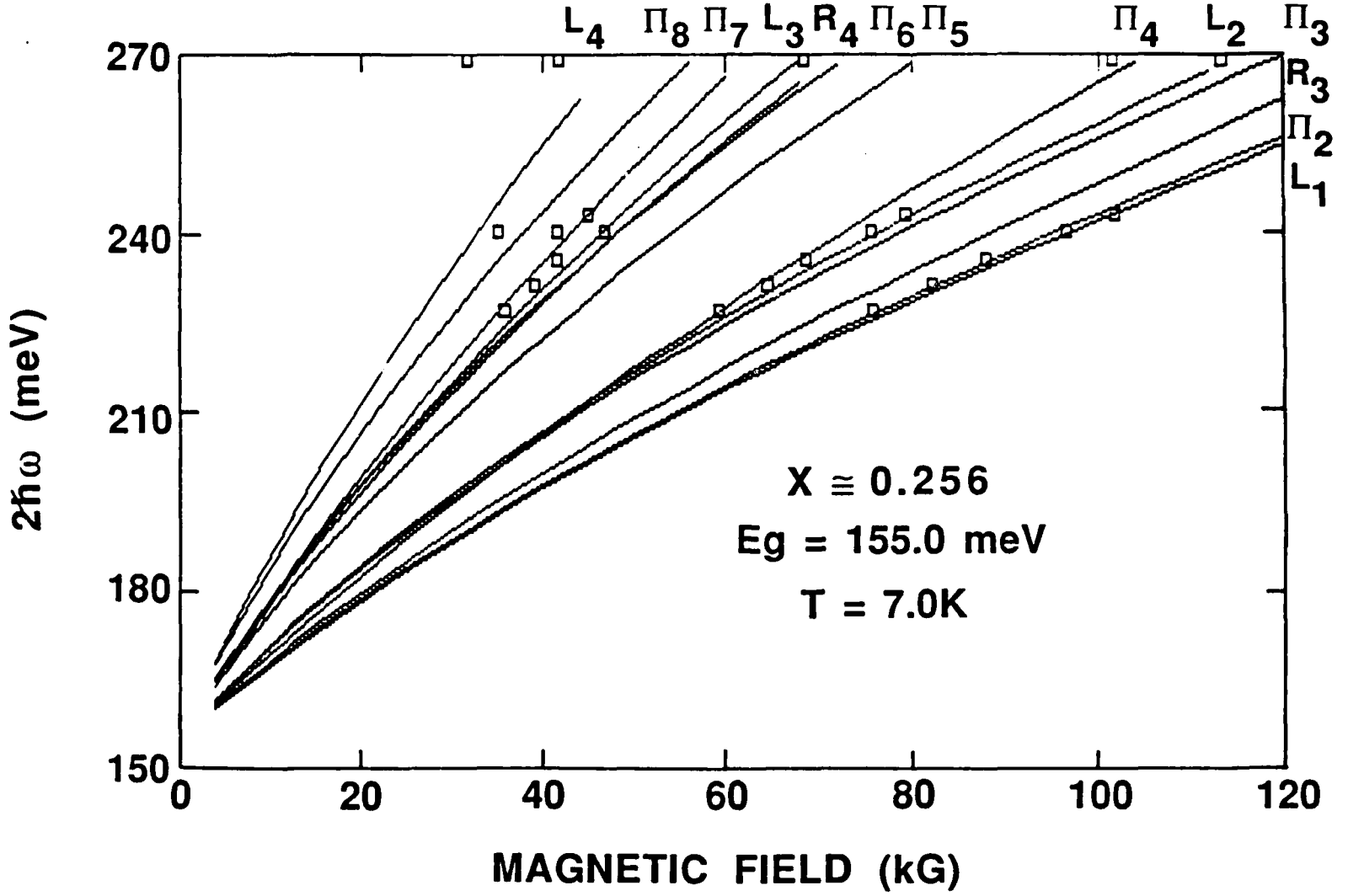

Figure 12. Fan chart of transition energies vs. magnetic field. The extrapolated band gap is 155.0 meV.

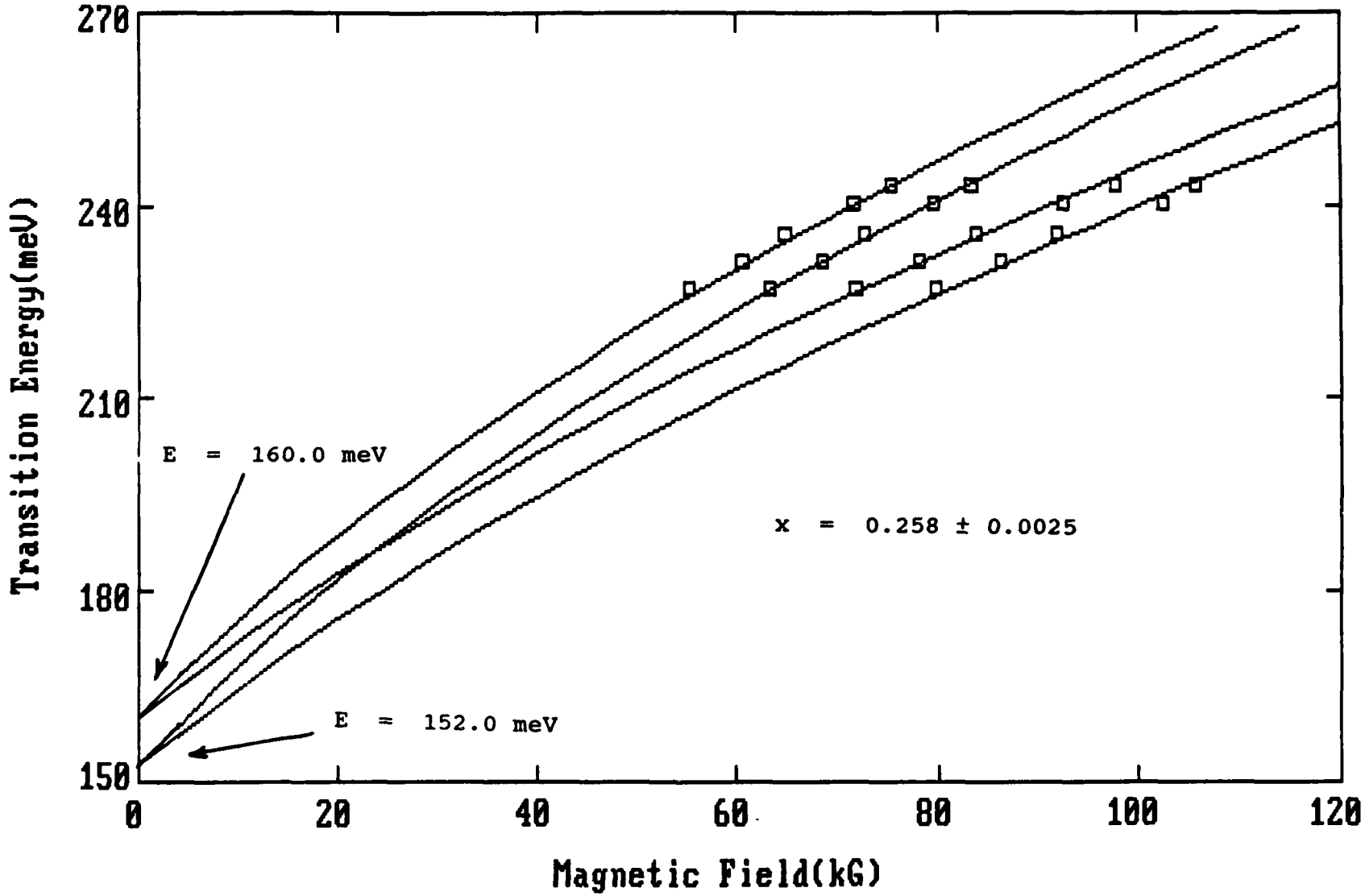

Figure 13. Fan chart of transition energy vs. magnetic field for the x = 0.258 sample. The typical full width at half max of the TPMA peaks was used as an estimate of the error. This analysis yields two band gap values which can be used to judge the relative accuracy of the x value throughout the sample.

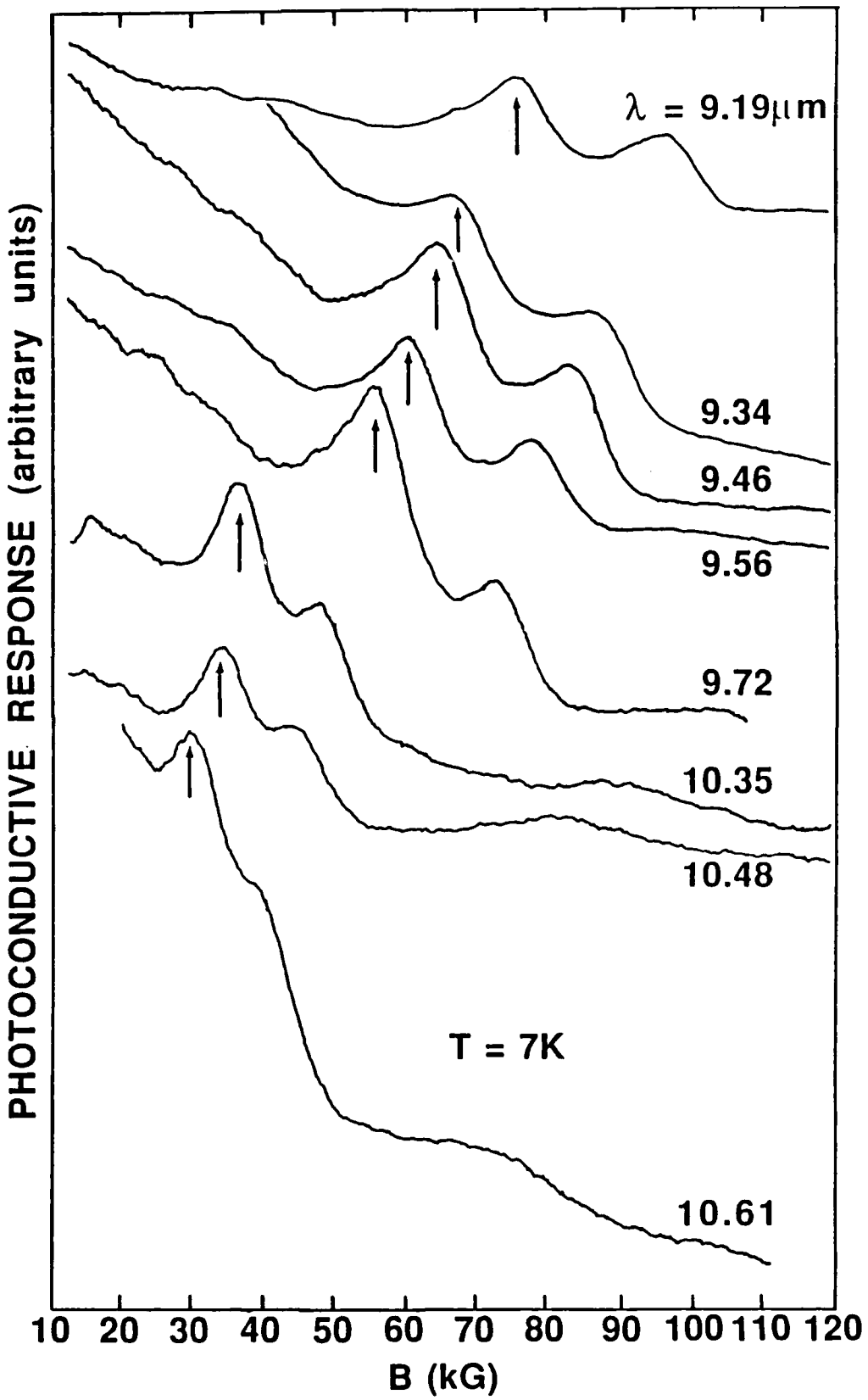

Figure 14. Photoconductive response vs. magnetic field for various wavelengths at 7 K. Note the two strong TPMA transitions.

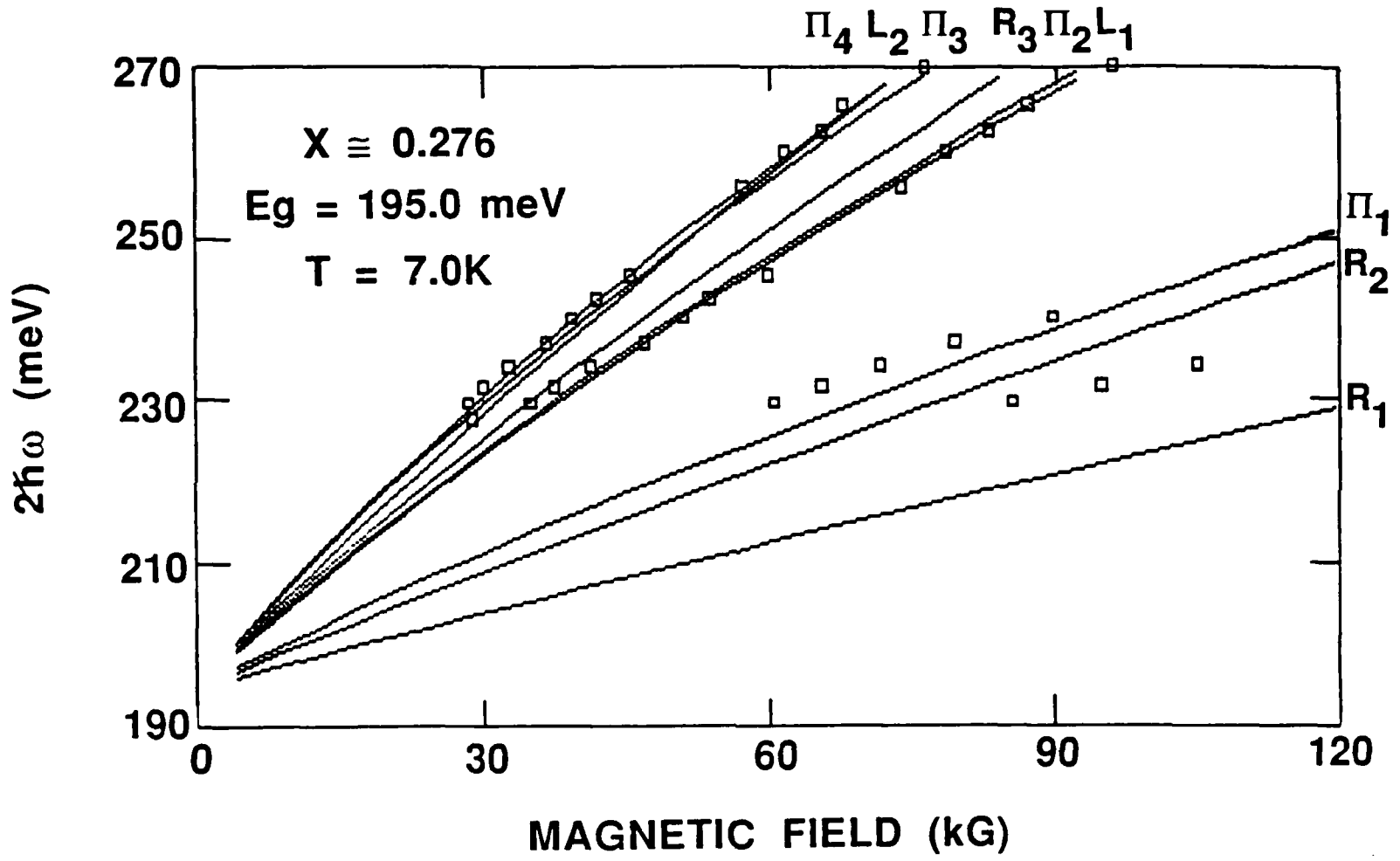

Figure 15. Fan chart of transition energies vs. magnetic field. The extrapolated band gap is 195.0 meV which yields an x value of 0.2811. The two transitions which do not lie along any theoretical line are believed to arise from mid-gap to conduction band transitions.

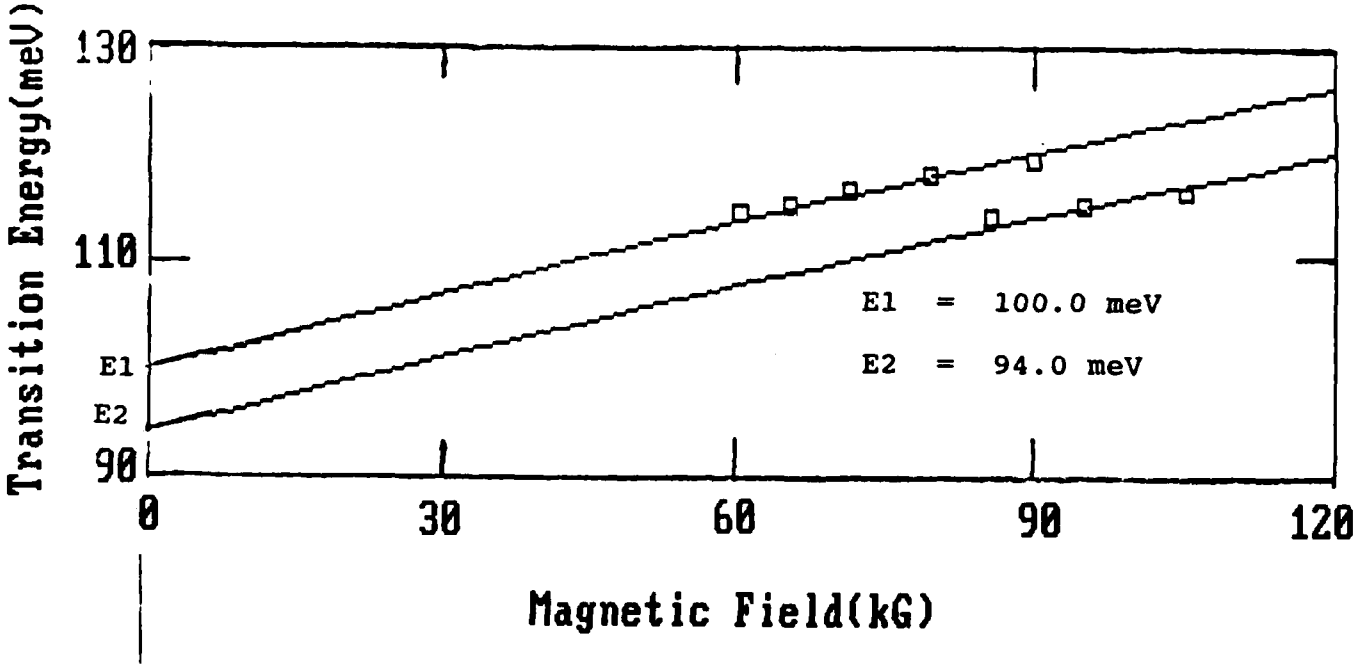

Figure 16. The two mid-gap to conduction band transitions fit with theoretical *Pidgeon-Brown calculations*. The two levels lie at 100 and 94 meV above the valence band.